

Classical and semiclassical description of Rydberg excitons in cuprous oxide

Jan Ertl,^{1,2} Patric Rommel,¹ Michel Mom,¹ Jörg Main,^{1,*} and Manfred Bayer²

¹*Institut für Theoretische Physik 1, Universität Stuttgart, 70550 Stuttgart, Germany*

²*Experimentelle Physik 2, Technische Universität Dortmund, 44221 Dortmund, Germany*

(Dated: June 17, 2020)

Experimental and theoretical investigations of excitons in cuprous oxide have revealed a significant fine-structure splitting of the excitonic Rydberg states caused by a strong impact of the valence band structure. We provide a semiclassical interpretation of that splitting by investigating the classical dynamics of the excitonic electron-hole pair beyond the hydrogen-like model. Considering the slow motion of Rydberg excitons in coordinate space compared to the fast dynamics of quasispin and hole spin we use an adiabatic approach and energy surfaces in momentum space for the computation of the exciton dynamics. We observe quasi-periodic motion on near-integrable tori. Semiclassical torus quantization yields the energy regions of the fine-structure splitting of n -manifolds in agreement with quantum mechanical computations.

Excitons in a semiconductor like cuprous oxide are created by the excitation of an electron from the valence band to the conduction band. The electron and the remaining hole in the valence band form a hydrogen-like system, which, however, is influenced by the band structure of the crystal. Since the early experiments on cuprous oxide by Gross [1] the experimental techniques have made enormous progress. In 2014 Kazimierzuk *et al.* realized the excitation of excitons with principal quantum numbers up to $n = 25$ for the yellow series in cuprous oxide [2]. These results have significantly inspired the field of giant Rydberg excitons. Due to the influence of the cubic O_h symmetry of the crystal, the exciton sequence shows deviations from a perfect hydrogen-like spectrum, viz. a fine-structure splitting of the n -manifolds [3, 4].

The complex band dispersion causing the fine-structure splitting can be described by introducing empirical quantum defects similar to the quantum defects in atoms [5]. The excitons are then described by a modified Rydberg formula, where the principal quantum number n is replaced by an effective quantum number $n_{\text{eff}} = n - \delta_{n,l}$. For the yellow exciton series the quantum defects $\delta_{n,l}$ are positive and grow with decreasing angular momentum l . They also slightly grow as function of n until saturating for large n . However, neither this phenomenological approach nor exact quantum computations for excitons provide the basis for an intuitive physical interpretation of the spectra. Similar is true for other complex systems, a prominent example being the hydrogen atom in a magnetic field, which is a quantum system, whose classical analogue shows a transition from regular to chaotic dynamics, and whose spectra in the non-perturbative regime can hardly be explained using a pure quantum mechanical terminology. Indeed, this system has become a prototype example for the investigation of *quantum chaos* by means of classical and semiclassical methods [6]. For the hydrogen atom semiclassical methods provide a deeper insight by, e.g., relating the energy spacing of Rydberg states to the periods of classical

Kepler orbits. To the best of our knowledge the classical dynamics of excitons and its relation to excitonic spectra has not yet been investigated. In particular it is an interesting question whether the influence of the band structure leads to regular, chaotic, or mixed regular-chaotic exciton dynamics.

In this Rapid Communication we use an adiabatic approach to compute the classical orbits of excitons in cuprous oxide including the complex valence band structure. We show that the classical exciton dynamics significantly deviates from the hydrogen-like model, and demonstrate that the fine-structure splitting of the n -manifolds can be interpreted via a semiclassical torus quantization of the quasi-periodic exciton orbits.

As mentioned above, a full description of excitons in cuprous oxide needs to consider the cubic O_h symmetry of the system. The uppermost valence band of cuprous oxide belongs to the irreducible representation Γ_5^+ [5, 7]. To consider this three-fold degenerate valence band one can introduce a quasispin $I = 1$. Additionally, the hole in the valence band has spin $S_h = 1/2$. Quasispin and hole spin are coupled by the spin-orbit term

$$H_{\text{SO}} = \frac{2}{3}\Delta \left(1 + \frac{1}{\hbar^2} \mathbf{I} \cdot \mathbf{S}_h \right), \quad (1)$$

where Δ is the spin-orbit coupling, and the components of the vectors \mathbf{I} and \mathbf{S}_h are the three spin matrices for $I = 1$ and $S_h = 1/2$, respectively. This leads to a splitting of the Γ_5^+ band into a higher lying two-fold degenerate Γ_7^+ band, connected to the yellow exciton series, and a lower lying four-fold degenerate Γ_8^+ band, connected to the green exciton series [5, 7, 8]. Introducing relative and center-of-mass coordinates for the electron and hole and neglecting the center-of-mass momentum, the Hamiltonian for excitons in cuprous oxide is given by [4, 9, 10]

$$H = E_g + \frac{\gamma'_1}{2m_0} \mathbf{p}^2 - \frac{e^2}{4\pi\epsilon_0\epsilon|\mathbf{r}|} + H_b(\mathbf{p}, \mathbf{I}, \mathbf{S}_h), \quad (2)$$

where the first term is the gap energy between the uppermost valence band and the lowest conduction band. The

second and third term correspond to the hydrogen-like model with $\gamma'_1 = \gamma_1 + m_0/m_e$ and the screened Coulomb potential with the dielectric constant ε . The fourth term

$$\begin{aligned}
H_b(\mathbf{p}, \mathbf{I}, \mathbf{S}_h) = & H_{\text{SO}} + \frac{1}{2\hbar^2 m_0} [4\gamma_2 \hbar^2 \mathbf{p}^2 \\
& - 6\gamma_2 (p_1^2 \mathbf{I}_1^2 + \text{c.p.}) - 12\gamma_3 (\{p_1, p_2\} \{\mathbf{I}_1, \mathbf{I}_2\} + \text{c.p.}) \\
& - 12\eta_2 (p_1^2 \mathbf{I}_1 \mathbf{S}_{h1} + \text{c.p.}) + 2(\eta_1 + 2\eta_2) \mathbf{p}^2 (\mathbf{I} \cdot \mathbf{S}_h) \\
& - 12\eta_3 (\{p_1, p_2\} \{\mathbf{I}_1 \mathbf{S}_{h2} + \mathbf{I}_2 \mathbf{S}_{h1}\} + \text{c.p.})], \quad (3)
\end{aligned}$$

accounts for the cubic band structure. Here, m_0 is the free-electron mass, $\{a, b\} = \frac{1}{2}(ab + ba)$ denotes the symmetrized product, c.p. stands for cyclic permutation, and the γ_i and η_i are the Luttinger parameters. In our computations we use the same material parameters as given in Ref. [11].

The Hamiltonian (2) can be treated in a quantum theoretical framework [4], where the lifting of the degeneracies of the Rydberg states can be observed. We want to provide a semiclassical interpretation for these phenomena by connecting the observed spectra to classical exciton orbits. Advancing to Rydberg states characterized by high principal quantum numbers, we make use of the Bohr correspondence principle to replace the operators for the relative motion by classical variables. In comparison to the hydrogen-like approach the band structure needs to be considered via quasispin and hole spin. With the Rydberg energy for the exciton $E_{\text{Ryd}} = 13.6 \text{ eV}/(\gamma'_1 \varepsilon^2) = 0.087 \text{ eV}$, the energy spacing $E_{\text{Ryd}}/n^2 - E_{\text{Ryd}}/(n+1)^2 \approx 2E_{\text{Ryd}}/n^3$ between adjacent Rydberg excitons is small compared to the spin-orbit coupling Δ already for Rydberg excitons with $n \geq 3$, which means that the characteristic timescale of the spin dynamics is short compared to that of the exciton dynamics in coordinate space. This allows for using an adiabatic approach by assuming that the fast spin dynamics reacts instantly to a change in the slow relative motion, in analogy to, e.g., the Born-Oppenheimer approximation for molecules, where the fast electron motion is assumed to react instantly to a slow change in the core configuration. In the following the spin dynamics and the exciton dynamics in coordinate space are treated quantum mechanically and classically, respectively.

As the hydrogen-like part of the Hamiltonian does not depend upon the spin quantum numbers, only the Hamiltonian (3) describing the band structure must be considered for the spin dynamics. The spin part of the wave function can be expanded in the basis $|m_I, m_{S_h}\rangle$ with m_I and m_{S_h} the magnetic quantum numbers of the quasispin and hole spin as

$$|\psi\rangle = \sum_{\substack{m_I=0,\pm 1 \\ m_{S_h}=\pm 1/2}} c_{m_I, m_{S_h}}(\mathbf{p}) |m_I, m_{S_h}\rangle. \quad (4)$$

The coefficients $c_{m_I, m_{S_h}}$ depend on the classical mo-

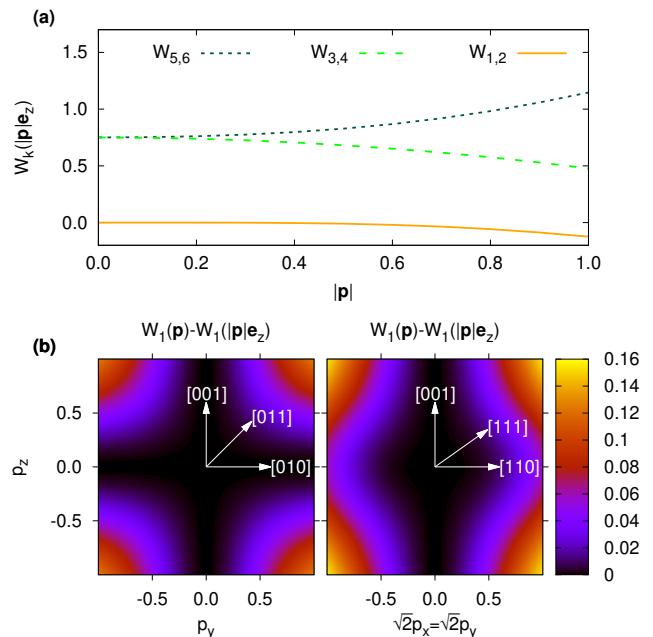


FIG. 1. (a) Energy surfaces related to the yellow and green exciton series along the [001] axis. (b) Energy surface $W_{1,2}(\mathbf{p})$ in the planes normal to the [100] (left) and $[1\bar{1}0]$ axis (right), respectively. For better visualization of the C_{4v} and C_{2v} symmetries the corresponding energy values along the z -axis $W_{1,2}(|\mathbf{p}|e_z)$ have been subtracted.

mentum \mathbf{p} of the exciton. Using the ansatz (4) in the Schrödinger equation $H_b(\mathbf{p}, \mathbf{I}, \mathbf{S}_h) |\psi\rangle = W |\psi\rangle$ and multiplying from the left with $|m'_I, m'_{S_h}\rangle$ leads to a six-dimensional Hermitian eigenvalue problem of the form

$$\mathbf{H}_b \mathbf{c} = W \mathbf{c}, \quad (5)$$

which can be numerically solved by an appropriate *LAPACK* routine [12]. A similar procedure was used for band-structure calculations in Refs. [5, 7]. The eigenvectors \mathbf{c} contain the coefficients from Eq. (4). The six eigenvalues W yield three distinct energy surfaces $W_k(\mathbf{p})$ that are two-fold degenerate due to Kramers theorem for half-integer spin systems with time-reversal symmetry. The energies along the [001] axis are shown in Fig. 1(a). In this figure and in the following all parameters are given in exciton-Hartree units which are obtained by setting $\hbar = e = m_0/\gamma'_1 = 1/(4\pi\varepsilon_0\varepsilon) = 1$.

When the quasispin and the hole spin are coupled to $\mathbf{J} = \mathbf{I} + \mathbf{S}_h$, the two energetically lowest surfaces $W_{1,2}(\mathbf{p})$ can be assigned to the approximate quantum number $J = 1/2$ associated with the yellow exciton series. The remaining energy surfaces can be assigned to $J = 3/2$ associated with the green exciton series [11]. The energy surfaces recover the cubic O_h symmetry of the system, i.e.,

$$W_k(O_h \mathbf{p}) = W_k(\mathbf{p}). \quad (6)$$

Cuprous oxide has two distinct classes of mirror planes. In the three planes normal to the [001] axis and its equivalents a C_{4v} symmetry can be recovered. The six planes normal to the [110] axis and its equivalents share the C_{2v} symmetry. The energy surfaces $W_{1,2}(\mathbf{p})$ for the yellow exciton series in the two distinct mirror planes are presented in Fig. 1(b). For a better visualization of their symmetry properties the energy values $W_{1,2}(|\mathbf{p}|e_z)$ along the z axis [see Fig. 1(a)] have been subtracted. Evidently, the C_{4v} and the C_{2v} symmetries of the corresponding planes in the crystal are recovered in the energy surfaces.

Replacing the term $H_b(\mathbf{p}, \mathbf{I}, \mathbf{S}_h)$ in Eq. (2) with one of the energy surfaces $W_k(\mathbf{p})$ corresponding to the yellow or green exciton series yields the Hamiltonian

$$\mathcal{H} = E_g + \frac{\gamma'_1}{2m_0} \mathbf{p}^2 - \frac{e^2}{4\pi\epsilon_0\epsilon|\mathbf{r}|} + W_k(\mathbf{p}), \quad (7)$$

which only depends on the exciton coordinates \mathbf{r} and momenta \mathbf{p} , and can therefore be utilized to calculate classical exciton orbits described by Hamilton's equations of motion

$$\dot{r}_i = \frac{\gamma'_1}{2m_0} p_i + \frac{\partial W_k(\mathbf{p})}{\partial p_i}, \quad \dot{p}_i = -\frac{e^2}{4\pi\epsilon_0\epsilon} \frac{r_i}{|\mathbf{r}|^3}. \quad (8)$$

Since the symmetry properties of the crystal are transcribed to the energy surfaces $W_k(\mathbf{p})$, classical orbits starting in one of the symmetry planes stay in that plane forever. In the following we focus on the yellow exciton series. The exciton orbits are calculated using algorithms for solving ordinary differential equations [13] and numerical root search [14]. The investigation of the classical exciton dynamics in the two-dimensional symmetry planes shows that the dynamics in the $(x=0)$ -plane perpendicular to the [100] axis is stable, i.e., orbits in that plane are robust against small perturbations of the x coordinate and the corresponding momentum. By contrast, the dynamics in the symmetry plane perpendicular to the [110] axis is unstable against perturbations out of the plane. In the following, we investigate the exciton dynamics in the stable $(x=0)$ -plane. The phase space structures can be visualized via a Poincaré surface of section (PSOS), where the phase-space coordinates (y, p_y) are plotted whenever the trajectory crosses the y axis, i.e., $z=0$. The PSOS at energy $E - E_g = -0.02$ (in exciton-Hartree units), which is related to an effective principal quantum number $n_{\text{eff}} \equiv [2(E_g - E)]^{-1/2} = 5$, is presented in Fig. 2(a). This energy lies, on the one hand, in a range with $n_{\text{eff}} > 3$ where the adiabatic approach discussed above is justified. On the other hand, quantum theoretical calculations are still feasible in this energy regime, and allow for the direct comparison of the quantum and semiclassical calculations. The PSOS shows an elliptical fixed point at about $y = 24.79$, $p_y = 0$ [blue dot in Fig. 2(a)], which is surrounded by near-integrable tori. Only in the outermost part of the PSOS

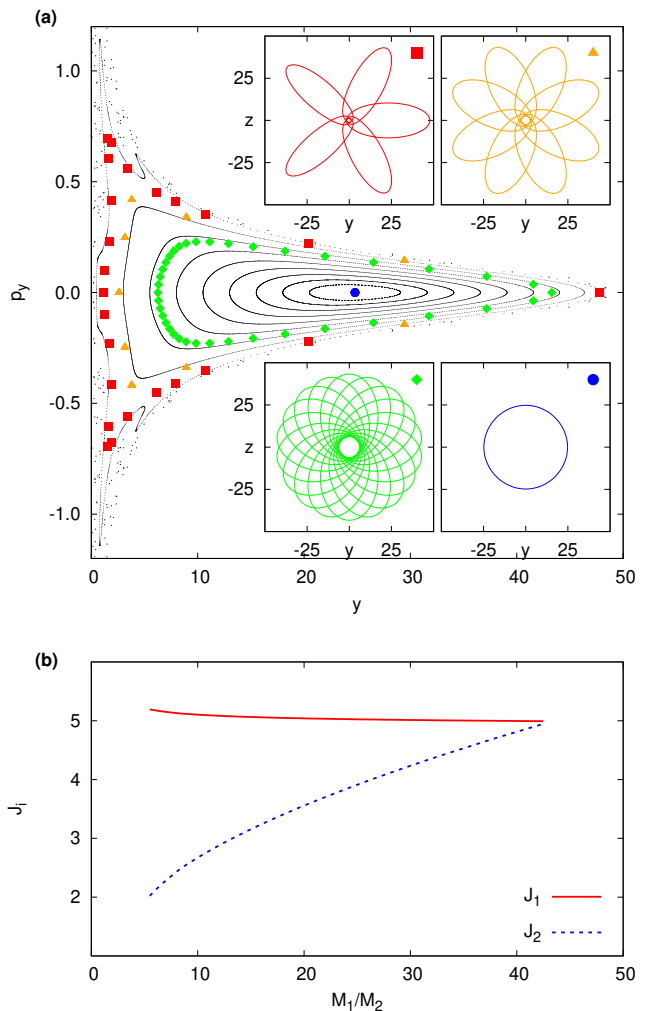


FIG. 2. (a) Poincaré surface of section (PSOS) of the orbits in the $(x=0)$ -plane at $n_{\text{eff}} = 5$. Dominating regular tori are surrounded by a small chaotic region. The insets show selected periodic orbits on rational tori marked with colored symbols. (b) Action variables J_1 and J_2 as functions of the ratio M_1/M_2 of the rotation numbers.

the torus structures break down, i.e., the points in this area are distributed stochastically. This indicates the onset of chaotic exciton dynamics in the overall mixed regular-chaotic phase space. Some selected rational tori are marked with colored symbols and the corresponding periodic orbits are shown as insets in Fig. 2(a). Qualitatively similar structures as for $n_{\text{eff}} = 5$ can be observed when the energy is varied. This will be discussed more detailed elsewhere.

The periodic orbits on the rational tori can be characterized by two integer rotation numbers (M_1, M_2) , where M_1 describes the number of Rydberg cycles of the orbit and M_2 is the number of rotations of these cycles around the x axis. The classical action of the periodic orbits is

given as

$$S_{M_1, M_2} = 2\pi M_1 J_1 + 2\pi M_2 J_2, \quad (9)$$

where J_1 and J_2 are the action variables of the torus, which smoothly depend on the energy and the ratio M_1/M_2 of the rotation numbers. The ratio M_1/M_2 increases from the outermost tori towards the central fixed point of the PSOS. This is related to a growing angular momentum of the classical orbits, i.e., orbits in the outermost (chaotic) part of the PSOS have low angular momenta and the nearly circular orbit belonging to the central fixed point has the highest angular momentum.

Using Eq. (9) and its derivative $dS_{M_1, M_2}/dM_1 = 2\pi J_1$, which can be well approximated by a differential quotient for two consecutive periodic orbits with rotation numbers M_1 differing by 1, the action variables J_1 and J_2 can be constructed for the rational tori and interpolated for the irrational tori. The action variables J_1 and J_2 at $n_{\text{eff}} = 5$ as function of the ratio M_1/M_2 are presented in Fig. 2(b). They behave monotonically in the finite region between $M_1/M_2 \approx 5.5$, which is close to the border of the regular tori [see Fig. 2(a)] and $M_1/M_2 \approx 43.5$ related to the central elliptical fixed point in the PSOS. For the nearly circular periodic orbit the two action variables coincide, i.e., it is $J_1 = J_2$ at the fixed point.

The action variables can in principle be used for a torus quantization to obtain semiclassical eigenvalues of the excitons. This, however, requires the extension of the two-dimensional torus discussed above to a three-dimensional torus with action variables (J_1, J_2, J_3) including the orbits out of the symmetry planes. Here we restrict ourselves to the quantization of the action variable J_1 , which then yields energy regions, where excitonic states with a given principal quantum number n can occur. As can be seen in Fig. 2(b), for fixed n_{eff} the values of the action variable J_1 related to allowed classical tori are restricted to a small and finite interval. The ratio of the rotation numbers connected to the outermost regular torus stays approximately at $M_1/M_2 = 5.5$ when increasing n_{eff} , whereas the ratio connected to the elliptical fixed point $(M_1/M_2)_{\text{max}}$ increases with increasing n_{eff} .

In Fig. 3 the J_1 intervals related to allowed classical tori are shown as a function of the effective quantum number n_{eff} . The green area marks the region of tori with ratio $5.5 < M_1/M_2 \leq (M_1/M_2)_{\text{max}}$ of the rotation numbers, which cover nearly all classical orbits except for those with very low angular momentum located in the outermost (chaotic) region of the PSOS [see Fig. 2(a)]. Semiclassical torus quantization requires $J_1 = n$ with $n = 1, 2, 3, \dots$ the principal quantum number. The intersection of these lines with the green area in Fig. 3 now yields the allowed regions for the fine-structure splitting of the n -manifolds, i.e., the intervals for the effective quantum number (and thus the energy), where exciton states with a given principal quantum number can exist.

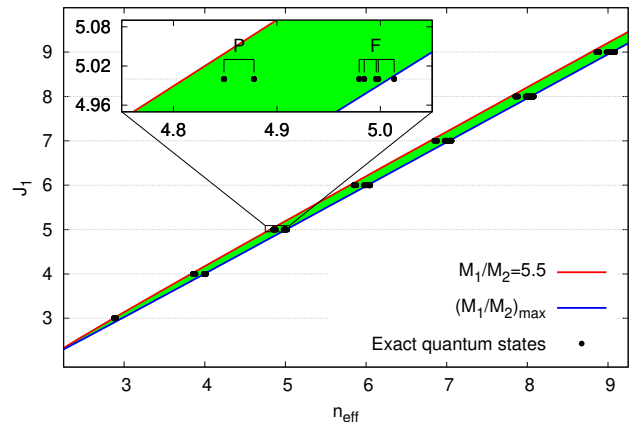


FIG. 3. Action variable J_1 as function of the effective quantum number n_{eff} . The green area marks the allowed region of tori with ratio M_1/M_2 of the rotation numbers between 5.5 (close to the outermost regular torus in the PSOS) and its maximum value $(M_1/M_2)_{\text{max}}$ (corresponding to the elliptical fixed point at the center of the PSOS). Semiclassically quantized exciton states belong to integer values of J_1 . The numerically exact quantum odd parity states with approximate principal quantum number n are marked by black dots. In the inset the region around $n = 5$ is enlarged and excitons are labeled as P (for $l = 1$) or F (for $l = 3$) states [3, 15]. The black dots are perfectly located on the intersections of the lines $J_1 = n$ with the green area of classical tori, which indicates the validity of the torus quantization for excitons.

To confirm the validity of the torus quantization we have computed the fine-structure splitting of excitons in cuprous oxide by diagonalization of the Hamiltonian using a complete basis set [4]. We restrict the calculations to the odd parity states because the even exciton series is dipole forbidden and cannot be observed in single photon experiments [2, 3]. Furthermore, the even excitons require the consideration of central-cell corrections [15], which are not included in our semiclassical approach. The exact exciton states of the odd parity n -manifolds with $n = 3$ to 9 are marked in Fig. 3 by black dots on the corresponding lines $J_1 = n$. They are perfectly located on the intersections of the lines $J_1 = n$ with the green area of classical tori. This clearly indicates the validity of the torus quantization for excitons. Approximate principal quantum numbers n and angular momentum quantum numbers L can be assigned to each exciton state of the yellow series [15], for $n = 5$ the dots are labeled as P or F excitons in the inset of Fig. 3. The F excitons appear at higher values of n_{eff} than the P excitons, in accordance with the analysis of the classical exciton dynamics as discussed above. The agreement of the semiclassical and quantum mechanical results in Fig. 3 is remarkable when considering the approximations, which have been used, i.e., the adiabatic approach for the quasispin and hole spin dynamics, the semiclassical approximation, and

the restriction of the classical exciton dynamics to one of the two-dimensional symmetry planes of the crystal.

In summary, we have investigated the classical exciton dynamics of cuprous oxide. The band structure of the crystal is taken into account via energy surfaces in momentum space, which are obtained using an adiabatic approach for the quasispin and hole spin. Orbits in the plane perpendicular to the [100] axis exhibit a quasi-periodic secular motion of Kepler ellipses on near-integrable tori in phase space. Semiclassical torus quantization allows for the interpretation of the fine-structure splitting of n -manifolds in terms of the classical exciton orbits. The obtained results thus lead to a deeper and more comprehensive physical understanding of excitons in semiconductors. Future work will include, e.g., the semiclassical computation of excitons based on the torus quantization of three-dimensional orbits, and the extension of the semiclassical approach to challenging energy regions of magnetoexcitons [16], where numerically exact computations are no longer feasible.

This work was supported by Deutsche Forschungsgemeinschaft (DFG) through Grant No. MA1639/13-1 and through the International Collaborative Research Centre (ICRC) TRR 160 (project A8). We thank Frank Schweiner for his contributions.

* Email: main@itp1.uni-stuttgart.de

- [1] E. F. Gross, *Il Nuovo Cimento* (1955-1965) **3**, 672 (1956).
- [2] T. Kazimierczuk, D. Fröhlich, S. Scheel, H. Stolz, and M. Bayer, *Nature* **514**, 343 (2014).
- [3] J. Thewes, J. Heckötter, T. Kazimierczuk, M. Aßmann, D. Fröhlich, M. Bayer, M. A. Semina, and M. M. Glazov, *Phys. Rev. Lett.* **115**, 027402 (2015).
- [4] F. Schweiner, J. Main, M. Feldmaier, G. Wunner, and C. Uihlein, *Phys. Rev. B* **93**, 195203 (2016).
- [5] F. Schöne, S.-O. Krüger, P. Grünwald, M. Aßmann, J. Heckötter, J. Thewes, H. Stolz, D. Fröhlich, M. Bayer, and S. Scheel, *Journal of Physics B: Atomic, Molecular and Optical Physics* **49**, 134003 (2016).
- [6] H. Friedrich and D. Wintgen, *Phys. Rep.* **183**, 37 (1989).
- [7] F. Schöne, S.-O. Krüger, P. Grünwald, H. Stolz, S. Scheel, M. Aßmann, J. Heckötter, J. Thewes, D. Fröhlich, and M. Bayer, *Phys. Rev. B* **93**, 075203 (2016).
- [8] G. Koster, J. Dimmock, R. Wheeler, and H. Statz, *Properties of the thirty-two point groups*, Massachusetts institute of technology press research monograph (M.I.T. Press, Cambridge, 1963).
- [9] C. Uihlein, D. Fröhlich, and R. Kenklies, *Phys. Rev. B* **23**, 2731 (1981).
- [10] N. O. Lipari and M. Altarelli, *Phys. Rev. B* **15**, 4883 (1977).
- [11] P. Rommel, P. Zielinski, and J. Main, *Phys. Rev. B* **101**, 075208 (2020).
- [12] E. Anderson, Z. Bai, C. Bischof, S. Blackford, J. Demmel, J. Dongarra, J. Croz, A. Greenbaum, S. Hammarling, and A. McKenney, *LAPACK Users' Guide, Third edition* (Society for Industrial and Applied Mathematics, Philadelphia, 1999).
- [13] W. Press, B. Flannery, S. Teukolsky, and W. Vetterling, *Numerical Recipes in FORTRAN 77: The Art of Scientific Computing. Second Edition* (Cambridge University Press, Cambridge, 1992).
- [14] J. J. Moré, B. S. Garbow, and K. E. Hillstom, *User guide for MINPACK-1*, Tech. Rep. (CM-P00068642, 1980).
- [15] F. Schweiner, J. Main, G. Wunner, and C. Uihlein, *Phys. Rev. B* **95**, 195201 (2017).
- [16] F. Schweiner, J. Main, G. Wunner, M. Freitag, J. Heckötter, C. Uihlein, M. Aßmann, D. Fröhlich, and M. Bayer, *Phys. Rev. B* **95**, 035202 (2017).